PAPER

Check for updates

A new dioxo-molybdenum complex derived from an amide-based imine derivative for the fluorescence recognition of Zr(IV) with phosphatase activity

Amit Kumar De,[a] Tandrim Shaym,[a] Subhasis Ghosh,[a] Sunanda Dogra,[b] Angshuman Roy Choudhury [iD] *[b] and Debasis Das [iD] *[a]

An amide-imine conjugate, namely, 2,4-dihydroxy-benzoic acid-(2-hydroxy-benzylidene)-hydrazide [DBASL], was prepared from 2,4-dihydroxy benzoic acid hydrazide (DBA) and salicylaldehyde and further used for the synthesis of the corresponding Mo(VI) complex (DBASLM). The structure of DBASLM was established using different spectroscopic techniques and confirmed by single-crystal X-ray diffraction (SC-XRD) analysis. Interestingly, DBASLM selectively recognizes ZrO^{2+} via 'turn-on' sky-blue emission, with notably strong binding constant of 1.3×10^5 M^{-1}. The proposed sensing mechanism involves the displacement of Mo(VI) from DBASLM by ZrO^{2+}. DFT studies also corroborate the interactions and allow the exploration of the associated orbital energy parameters. Silica-immobilized DBASLM is very effective for the solid-phase extractive separation/recovery of ZrO^{2+}. A DBASLM-impregnated paper strip allows the low-cost, facile and instant optical detection of ZrO^{2+} in real samples. DBASLM promotes phospho-ester bond hydrolysis in p-nitrophenyl phosphate (p-NPP), which is one of the vital biological processes that play a key role in the destruction of poisonous organo-phosphorus substrates such as pesticides and insecticides used in the agricultural industry.

Introduction

Zirconium (Zr) has pervasive applications in different fields, such as metallurgy, materials science, aerospace, atomic energy, medicine, and petrochemicals.[1] Its valuable attributes include corrosion resistance and enhancement of mechanical strength of alloys that function over a wide range of temperatures.[2–4] Zr materials have also been used extensively in artificial internal organs in the last few years[5–7] as they offer low toxicity with excellent bio-compatibility.[8,9] However, the risks involved in the use of Zr compounds depend on various factors such as the concentration, duration of exposure, and chemical form.[10–12] Frequent contact with high-concentration Zr compounds may result in health issues such as pulmonary granuloma, skin irritation, carcinogenesis, and hypersensitivity pneumonitis.[13–19] The National Institute for Occupational Safety and Health (NIOSH) has proposed the maximum exposure limit for Zr compounds as 5 mg L^{-1} for an 8 h workday, while it is 10 mg L^{-1} for short-term exposure.[8]

Given that Zr(IV) sensors are relatively scarce, ample opportunity exists to develop probes for the rapid and inexpensive detection of Zr(IV). Among the various techniques and methods for its detection, which depend on several factors including concentration range, sample matrix, sensitivity and selectivity, the fluorescence method is superior and therefore in high demand.[20]

On the other hand, phospho-ester bond cleavage, one of the vital biological processes, plays a key role in the destruction of poisonous organo-phosphorus substrates such as pesticides and insecticides used in the agricultural industry.[21–27] Eventually, they accumulate in humans via the food chain, causing harmful effects.[22,23,28–30]

Considering the above-mentioned two facts, we have attempted to prepare materials that can serve both purposes, which are rarely found in the literature. Recently, a few probes have been reported that can selectively detect and determine Zr(IV) in acid media.[31–33] Herein, we report a fluorescence probe (DBASLM) that can selectively detect Zr(IV) at neutral pH in the form of ZrO^{2+} via 'turn-on' sky-blue fluorescence ($\lambda_{ex} = 278$ nm and $\lambda_{em} = 477$ nm) having the lowest limit of detection (LOD) of 23.1 nM and binding constant of 1.3×10^5 M^{-1}. In addition, DBASLM efficiently cleaves the phospho-ester bond in poisonous organo-phosphorus substrates (p-nitrophenyl phosphate, p-NPP).

[a]Department of Chemistry, The University of Burdwan, Burdwan-713104, WB, India. E-mail: ddas100in@yahoo.com

[b]Department of Chemical Sciences, Indian Institute of Science Education and Research (IISER), Knowledge City, Sector 81, S.A.S. Nagar, Manauli P.O., Mohali, Punjab, 140306, India

Experimental

Synthesis (Scheme 1)

2,4-Dihydroxybenzoic acid hydrazide (DBA). Employing the materials mentioned in the SI, a few drops of thionyl chloride (SOCl$_2$) were added to an ethanol solution of 2,4-di-hydroxybenzoic acid (0.80 g, 5.19 mmol) under stirring conditions at room temperature (Scheme 1). The resulting solution was reacted with hydrazine hydrate to obtain the corresponding hydrazide (DBA) in 68% yield. Its molecular formula is C$_7$H$_8$N$_2$O$_3$ (M.W. = 168.15). Anal. found (%), C, 49.70; H, 4.50 and N, 16.80; calcd (%), C, 50.00; H, 4.80 and N, 16.66. ESI-MS (m/z) [M + H]$^+$, 169.0247; [M + Na]$^+$, 191.0012 (Fig. S1a, SI). ^{1}HNMR (Fig. S1b, SI), 400 MHz, DMSO-d_6, TMS, J (Hz), d (ppm): 12.76 (1H, s), 10.07 (1H, s), 9.78 (1H, s) 7.65–7.63 (1H, d, J = 8.40), 6.29–6.25 (2H, q), 4.54 (2H, s). ^{13}CNMR (Fig. S1c, SI) [100 MHz, DMSO-d_6, TMS, d (ppm)]: 169.14, 162.81, 128.81, 107.55, 106.17, 103.20, and 39.88. FT-IR (KBr, cm^{-1}): 3390, v(O–H); 3230, v(N–H); 3099, v(C–H, aromatic); 1622, v(C=O); 1050, v (N–N) (Fig. S1d, SI).

2,4-Dihydroxy-benzoic acid-(2-hydroxy-benzylidene)-hydrazide (DBASL). A mixture of DBA (170 mg, 1.01 mmol) and salicylaldehyde (123 mg, 1.01 mmol) in methanol (10 mL) was refluxed for 4 h and the resulting solution was left undisturbed for slow evaporation to yield white DBASL after 2 days in 89% yield (Scheme 1). Its molecular formula is C$_{14}$H$_{12}$N$_2$O$_4$ (M.W. = 272.26). Anal. found (%), C, 61.30; H, 4.72 and N, 10.81; calcd (%) C, 61.76; H, 4.44 and N, 10.29. ESI-MS (m/z) [M + H]$^+$, 273.0574; [M + Na]$^+$, 295.0352 (Fig. S2a, SI). ^{1}HNMR (DMSO-d_6, 400 MHz, J Hz, d ppm) 12.26 (1H, s), 11.92 (1H, s), 11.28 (1H, s), 10.31 (1H, s), 8.66 (1H, s), 7.83–7.80 (1H, d, J = 8.8 Hz), 7.56–7.54 (1H, d, J = 6.8), 7.32–7.29 (1H, t), 6.95–6.91 (2H, q), 6.41–6.34 (2H, m) (Fig. S2b, SI). ^{13}CNMR (Fig. S2c, SI) [100 MHz, DMSO-d_6, TMS, d (ppm)]: 165.59, 163.36, 162.68, 157.93, 148.82, 131.91, 130.25, 129.97, 119.83, 119.12, 116.90, 108.07, 106.38, 103.33, and 40.15. FT-IR (KBr, cm^{-1}): 3400, v(O–H); 3080, v(C–H, aromatic); 1653, v(–CH=N); 1621, v(C=N); 1084, v(N–N) (Fig. S2d, SI).

DBASLM. A mixture of MoO$_2$(acac)$_2$ (0.4 g, 1.23 mmol, EtOH : DMF, 2 : 3, v/v) and DBASL (0.312 g, 1.15 mmol, 10 mL
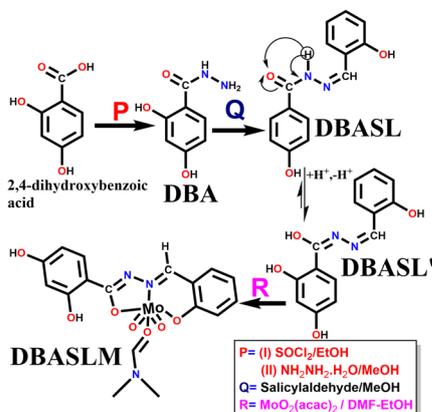
EtOH) was stirred for 2 h and left undisturbed for slow evaporation to yield orange crystals of DBASLM in 58% yield, molecular formula C$_{20}$H$_{24}$MoN$_4$O$_8$ (M.W. = 544.37). Anal. found (%), C, 43.91; H, 4.70 and N, 11.11; calcd (%) C, 44.06; H, 4.57 and N, 10.28. ESI-MS (m/z): [M + H]$^+$, 474.0879 [including one DMF present in its crystal lattice] (Fig. S3a, SI). FT-IR (KBr, cm^{-1}): 3404, v(O–H); 3082, v(C–H, aromatic); 1651, v(–CH=N); 1610, v(C=N)-imide; 1070, v(N–N) (Fig. S3b, SI). The structure of DBASLM is confirmed by SC-XRD analysis.

DBASLZ from DBASLM. A freshly prepared ethanol solution of ZrO(NO$_3$)$_2$ (1 M) was added drop-wise to an aqueous ethanol (EtOH : H$_2$O, 1 : 2, v/v) solution of DBASLM (1 M) under stirring conditions. The resultant mixture was left undisturbed for slow evaporation of the solvent to get yellow-green DBASLZ in 48% yield, molecular formula C$_{14}$H$_{14}$N$_2$O$_7$Zr (M.W. = 413.49). Anal. found (%), C, 40.37; H, 3.46 and N, 6.82; calcd (%) C, 40.67; H, 3.41 and N, 6.77. ESI-MS (m/z): [M + H]$^+$, 414.0481 (Fig. S4a, SI). FT-IR (KBr, cm^{-1}): 3406, v(O–H); 3078, v(C–H, aromatic); 1645, v(–CH=N); 1608, v(C=N)-imide; 1065, v(N–N) (Fig. S4b, SI).

Results and discussion

Single-crystal X-ray diffraction analysis

The molecular structure of DBASLM (CCDC No. 2448883) has been authenticated by single-crystal X-ray diffraction analysis and presented in Fig. 1 and its packing diagram in Fig. S5a (SI). Its crystallographic parameters [triclinic, space group: P1, volume (Å^3): 1132.43(7); Z = 2] are presented in Table S1 (SI). Selected bond lengths and bond angles are presented in Table S2 (SI). The geometry of DBASLM is distorted octahedral (Fig. 1). The bond lengths of O3–C1 [1.327(3) Å] for the amide C–O bond and O7–C10 [1.360(3) Å] for the phenol C–O bond are close and signify single-bond character (Fig. S5b, SI). The partial double-bond character is reflected by the bond lengths of N1–C1 [1.307(3) Å], N2–C8 [1.288(3) Å], N1–N2 [1.392(3) Å], C1–C2 [1.465(4) Å] and C8–C9 [1.448(4) Å]. Two Mo=O groups, viz. Mo–O4 [1.693(2) Å] and Mo–O6 [1.711(2) Å] are in the cis-geometry and indicate double-bond character. On the other hand, the bond lengths of Mo1–O3 [2.007(2) Å], Mo–O7 [1.932(2) Å], and Mo–O5 [2.322(2) Å] indicate Mo–O single-bond character. The solvent DMF coordinated to Mo(vi) via the carbonyl oxygen (–O5). The bond angles of O3–Mo–O7 [149.35(6)°], O4–Mo–O5

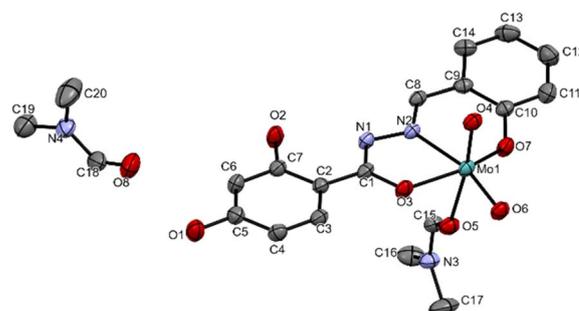**Scheme 1** Synthesis of DBA, DBASL and DBASLM.

Fig. 1 Thermal ellipsoid plot of the asymmetric unit of DBASLM, where H atoms are excluded for clarity.

[171.59(9)°] and O6–Mo–N2 [162.6(1)°] indicate that DBASLM exhibits a distorted octahedral geometry.

Spectroscopic studies

DBASL interacts with common cations such as Zn^{2+}, Cd^{2+}, Al^{3+}, ZrO^{2+}, La^{3+} and Y^{3+} to produce fluorescence (Fig. S6a, SI). The interaction of DBASLM with common cations, including rare-earth ions, viz., K^+, Na^+, Fe^{2+}, Mg^{2+}, Mn^{2+}, Ni^{2+}, Zn^{2+}, Ca^{2+}, Cd^{2+}, Co^{2+}, Cu^{2+}, Al^{3+}, Cr^{3+}, Fe^{3+}, ZrO^{2+}, Ce^{4+}, Dy^{3+}, Gd^{3+}, La^{3+}, Nd^{3+}, Sm^{3+} and Y^{3+} (as nitrate salts), have been studied in different common media, namely, MeOH, EtOH, propanol, DMSO and THF (Fig. S6b–n, SI, respectively). It is found that DBASLM selectively recognizes ZrO^{2+} in EtOH–H_2O (3 : 7, v/v). DBASLM exhibits a higher emission intensity at $\lambda_{ex} = 278$ nm in the presence of ZrO^{2+} in an ethanol–water system (Fig. S6o–q, SI). It is interesting to note that the emission intensity of the system decreases with an increasing water percentage in aqueous ethanol (Fig. S7a, SI). Interference from Y^{3+} may be eliminated using Na_2EDTA (Fig. S8a and b, SI). Moreover, the emission intensity of the probe in the presence and absence of ZrO^{2+} varies with pH (Fig. S9, SI). The optimum sensing efficiency has been observed at around pH 7, which was maintained in all experiments using PBS buffer.

Absorption spectroscopic studies

Studies on the spectroscopic interaction of common cations (mentioned supra) with DBASLM were performed in EtOH–H_2O (3 : 7, v/v) media. The parent ligand, DBASL, absorbs at 335 nm, which is almost the same in different solvents (Fig. S9a, SI).
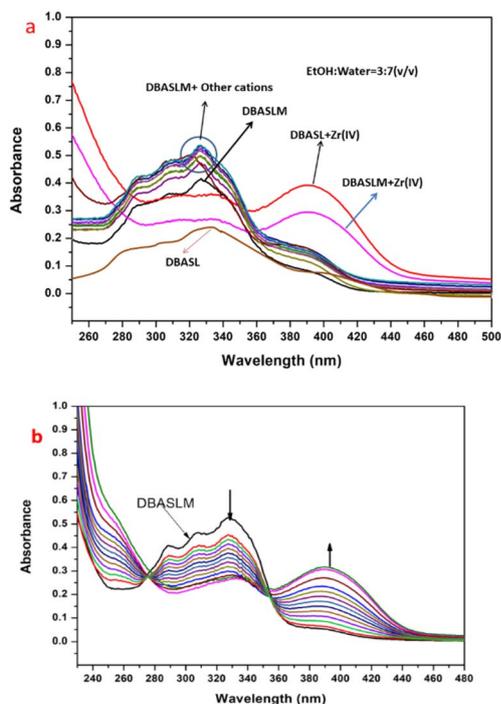
Upon the addition of Mo(vi) to DBASL, its absorbance increases significantly with a minor blue shift to 327 nm (Fig. 2a), reflecting the notable interaction between DBASL and Mo(vi).

On the other hand, upon the gradual addition of ZrO^{2+} to DBASLM, its absorbance at 327 nm decreases notably, while a new peak appears at 391 nm, along with an isosbestic point at 353 nm (Fig. 2b). This is attributed to the displacement of Mo(vi) from DBASLM by ZrO^{2+}.

Emission spectroscopic studies

The addition of ZrO^{2+} to DBASLM results in an intense sky-blue emission at 477 nm ($\lambda_{ex} = 278$ nm, Fig. 3a) (Fig. S7b, SI). Although most other common cations (mentioned supra) remain silent towards DBASLM, Y^{3+} enhances its fluorescence to some extent (Fig. S10, SI), and also interferes to some extent in a competitive environment (Fig. S11, SI). The emission intensity of DBASLM is gradually enhanced upon the addition of ZrO^{2+} (Fig. 3b).

Job's plot discloses a 1 : 1 stoichiometry (mole ratio) for the [DBASLM–ZrO^{2+}] adduct (Fig. S12a, SI), which is also supported by mass spectra. The binding constants for DBASLM and DBASL for ZrO^{2+} were determined using the Benesi–Hildebrand equation (considering 1 : 1 binding, Fig. S12b and d, SI, respectively). The corresponding LOD values for ZrO^{2+} were calculated using Fig. S13b and d, respectively (SI) and presented in Table 1. The plot of emission intensity of DBASLM vs. ZrO^{2+} is linear up to 23.1 nM ZrO^{2+} (Fig. S14, SI) and useful for the determination of an unknown ZrO^{2+} concentration. The effect of solvents reveals that its emission intensity is higher in polar protic coordinating solvents such as MeOH, EtOH, and propanol, while a lower
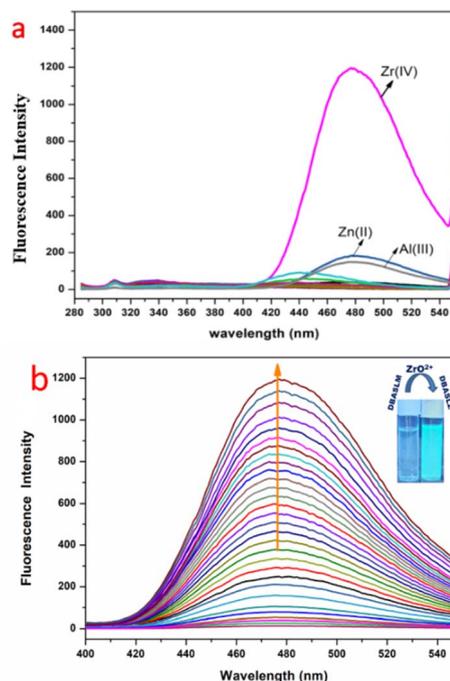

Fig. 2 Changes in the absorption spectra of DBASL and DBASLM (50 μM) upon the addition of (a) common cations [1500 μM] and (b) ZrO^{2+} [0–1000 μM] in EtOH–H_2O (3 : 7, v/v, PBS buffer, pH 7.0).

Fig. 3 Changes in the emission spectra of DBASLM (50 μM) upon the addition of (a) common cations (supra) [1500 μM] and (b) ZrO^{2+} [0–3000 μM] in EtOH–H_2O (3 : 7, v/v, PBS buffer).

Table 1 Binding constants and LODs of DBASLM and DBASL for ZrO^{2+} in EtOH–H$_2$O (3 : 7, v/v)

Probe	Binding constant (M^{-1})	LOD (nM)
DBASLM	1.3×10^5	23.1
DBASL ligand	1.5×10^5	21.9

intensity is observed in polar aprotic coordinating solvents such as DMSO and THF at relatively shorter wavelengths. On the other hand, in non-coordinating solvents such as CCl$_4$, CHCl$_3$, and CH$_2$Cl$_2$, no emission is observed (Fig. S6c, SI). These observations are in line with the literature that the emission intensities and excitation wavelengths are both influenced by the solvent polarity.

Sensing mechanism

The weak emissions of DBASL are attributed to the photo-induced electron transfer (PET) process that arises from its amide –N to –CH=N-portions. Mo(VI) inhibits the PET and –CH=N-isomerisation, although the anticipated fluorescence enhancement is absent, which depends on several factors such as the nature of the metal ion and its oxidation state and electronic energy levels. Interestingly, only in the presence of ZrO^{2+}, both the parent DBASL and the probe (DBASLM) experience a fluorescence enhancement (Fig. S7b, SI). One reason for this may be the comparatively lower charge of Zr(IV) over Mo(VI), which shows CHEF in the case of DBASL, while the other one is the selective replacement of Mo(VI) in DBASLM by ZrO^{2+}, which may have several reasons for its better fit. It should be noted that almost similar absorption and emission profiles (Fig. 2a and S7b, SI) were observed when ZrO(NO$_3$)$_2$ was added separately to DBASL and DBASLM solutions. The ESI-MS (m/z) spectrum and single-crystal X-ray structure support the formation of DBASLM. In brief, the addition of ZrO^{2+} turns the fluorescence of DBASLM ON, which is attributed to the metal displacement process, where Mo(VI) is replaced by ZrO^{2+} due to the formation of strong Zr–O and Zr–N bonds,[31,34,36,37] resulting in [DBASL–Zr(IV)] (DBASLZ, Scheme 2).[38,39] This is reflected in the corresponding ESI-MS spectrum, having (m/z) of $[M + H]^+ = 414.0481$. Job's plot also suggests the formation of a 1 : 1 complex (Fig. S12a, SI). The sensing protocol is further substantiated by ^{1}HNMR spectroscopy and DFT studies.
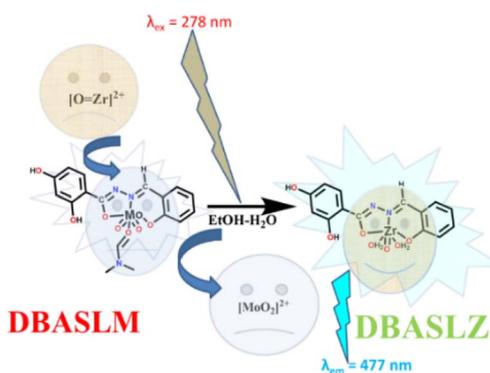
Scheme 2 Interaction mode of ZrO^{2+} with DBASLM.
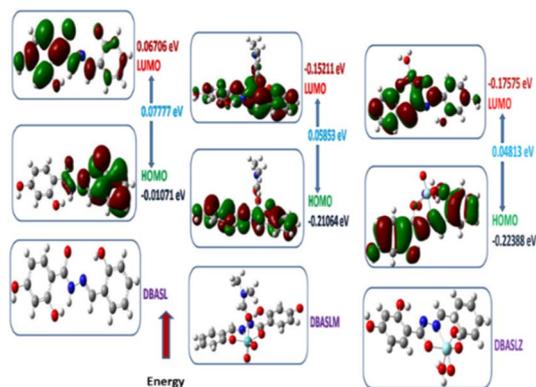
Fig. 4 Frontier molecular orbitals (HOMO–LUMO) with the energies of DBASL, DBASLM and DBASLZ.

Fig. 5 UV light-irradiated view of ZrO^{2+}-sorbed DBASLM-immobilized silica.

^{1}HNMR spectral studies

The ^{1}HNMR spectral studies reveal the mode of binding of DBASLM with ZrO^{2+}. Upon the addition of MoO$_2$(acac)$_2$ (1.0 equiv.) to DBASL, the protons of the phenol –OH in the salicylaldehyde moiety (c, 11.280 ppm) and imidic (d, 10.321 ppm) acid moiety disappear.[37] The imine proton (e, 8.655 ppm) also shifted downfield to 8.661 ppm. On the other hand, when ZrO^{2+} (1.0 equiv.) was added to the DBASLM complex, the peaks for the phenol –OH proton (c, 11.280 ppm) and imidic acid (d, 10.321 ppm) were still absent. The imine proton (e, 8.655 ppm) also shifted downfield to 8.723 ppm (Fig. S4c, SI).[34,35]
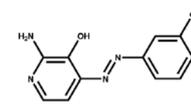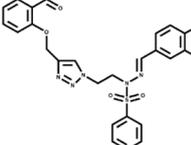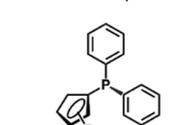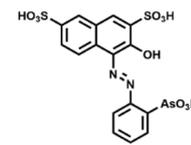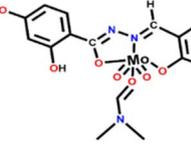
DFT studies

The theoretical energy parameters of the corresponding frontier molecular orbitals in the process of probe-analyte interaction were computed by density functional theory (DFT) studies.[40] DFT was performed with DBASL, DBASLM, and DBASLZ molecule/complex/

Table 2 Solid-phase extraction of ZrO^{2+} using silica-immobilized DBASLM

Test	ZrO^{2+} added (10^{-2} M)	Found (10^{-2} M)	Recovery (%)
1	8.85	6.43	72.90 ± 1.08
2	10.60	7.42	70.00 ± 1.25
3	12.80	8.48	66.25 ± 1.35

Table 3 Comparison of DBASLM with the reported probes

Sl. No.	Probe	Method	pH	LOD (nM)	Ref.
1	Phosphorylated and pyrene-labeled oligonucleotides	Fluorescence	7.4	200	46
2	Histidine-functionalized gold nanoparticles	Colorimetric and chrominance	7.0	2620 and 6250	47
3		Colorimetric	6.5	82.23	31
4		Colorimetric and fluorescence	Non-aqueous medium	50 and 0.90	34
5		Potentiometric	4.8	18	48
6		PVC membrane-based electrode	1.8–4.2	600	49
7		Fluorescence	7.0	23.1	Present work

adduct using the TD-SCF/DFT/B3LYP/6-31G(d) (for C, H, N and O) and LANL2DZ (for Mo and Zr) basis sets.[41] The energy gaps between the highest occupied molecular orbitals (HOMO) and lowest unoccupied molecular orbitals (LUMO) for DBASL, DBASLM and DBASLZ are important parameters (Fig. 4). The energy difference between the HOMO–LUMO for DBASL is 0.07777 eV, where the HOMO–LUMO energy gap for DBASLM decreased by 0.01924 eV. The corresponding value for DBASLM is 0.05853 eV, indicating the stability of the complex. The related energy difference for the DBASLZ adduct is 0.04813 eV. Here, a slight decrease in the energy gap for DBASLM by 0.01040 eV and DBASL by 0.02964 eV is observed. Moreover, the HOMO and LUMO energies also decreased in the same order from DBASL to DBASLZ *via* DBASLM. Therefore, the addition of ZrO^{2+} to DBASLM lowers the HOMO–LUMO energy gap and is associated with a red shift, demonstrating that the experimental observations match the theoretical values.[37]

Solid-phase extraction

For the immobilization of DBASLM on silica (100–200 mesh), 1.8 g DBASLM and 8.5 g silica (100–200 mesh) were mixed and refluxed for 4 h in methanol.[42,43] After removal of the solvent, DBASLM immobilized on silica was obtained.[42,43] A glass column (10 cm × 1 cm) was filled with the DBASLM-immobilized silica to a height of
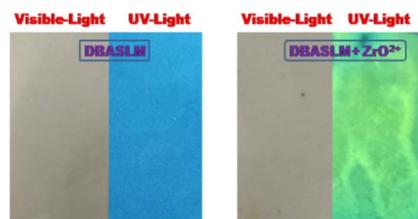

Fig. 6 DBASLM-soaked paper strip for the detection of ZrO^{2+}.

approximately 7 cm. A real water sample spiked with $ZrO(NO_3)_2$ was passed through the column at a flow rate of 1 mL min⁻¹. Upon exposure to UV light, the colour of the silica bed changed to sky blue, indicating the sorption of ZrO^{2+} (Fig. 5). The sorbed ZrO^{2+} could be eluted by a DCM–ethyl acetate (3/7, v/v) mixture. After evaporating the solvent, the residue was used to prepare a solution in EtOH–H_2O and the concentration of ZrO^{2+} was measured following the developed method (Table 2). Comparison of the present probe with existing pioneering ZrO^{2+} selective probes are presented in Table 3.

Visualization of ZrO^{2+} on a paper strip soaked with DBASLM

The paper strip method for the visualization of ZrO^{2+} utilizing DBASLM is cost-effective and instanteneous.[44,45] A drop of ZrO^{2+}

Paper
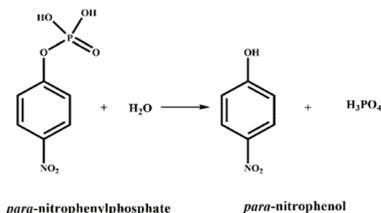
Scheme 3 Hydrolysis of *p*-NPP using DBASLM as a catalyst.
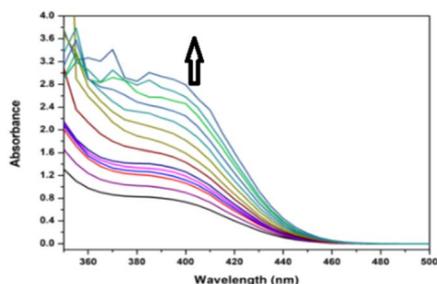
Fig. 7 Changes in the absorption spectrum of *p*-NPP upon the addition of DBASLM.

Table 4 Rate constants for the hydrolysis of *p*-NPP in the presence and absence of DBASLM/DBASL

Substrate	Catalyst	Rate constant (s^{-1})
p-NPP (0.02–10.0 mmol)	Blank	1.86×10^{-5}
p-NPP (0.02–10.0 mmol)	DBASL (0.01 mmol)	4.00×10^{-5}
p-NPP (0.02–10.0 mmol)	DBASLM (0.01 mmol)	1.84×10^{-4}

solution was placed on a colourless paper strip soaked with DBASLM and air dried. Sky-blue emission was observed upon the irradiation of the above-mentioned paper strip with UV light, indicating the presence of ZrO^{2+} (Fig. 6).

Studies on *p*-nitrophenyl-phosphate (*p*-NPP) activity

Phosphoester bond hydrolysis of *p*-nitrophenyl phosphate (*p*-NPP) is a very slow process, but its reaction rate (Scheme 3) may be enhanced using a catalyst.[30,50,51] In the present case, a catalytic amount of DBASLM (0.4 mmol, 10 mol% relative to *p*-NPP) was reacted with *p*-NPP (4.0 mmol) in MeOH–H$_2$O (1 : 4, v/v, pH 7, PBS buffer) and an increase in absorbance at 410 nm was observed with time due to the formation of yellow *p*-nitrophenol (Fig. 7).[50] The proposed mechanism is supported by the QTOF mass spectra with the *m/z* value of 139.0286 (calcd *m/z*: 139.11) (Fig. S15, SI).[52] The absorbance *vs.* time plot revealed the progress of the reaction (Fig. S16, SI).[53] The hydrolysis rate constants derived from Fig. S17 (SI) at 25 °C are presented in Table 4.

Conclusion

An amide-imine (DBASL)-derived Mo(IV) complex, structurally authenticated by single-crystal X-ray diffraction analysis, has

been employed for the selective recognition of ZrO^{2+} [Zr(IV)] *via* its sky-blue ($\lambda_{em} = 477$ nm and $\lambda_{ex} = 278$ nm) emission in aqueous EtOH media. Its sensing is attributed to the displacement of Mo(VI) from DBASLM by ZrO^{2+}, resulting in sky-blue fluorescence. The limit of detection for DBASLM for ZrO^{2+} is 23.1 nM. Silica-immobilized DBASLM is effective for the solid-phase extractive recovery of ZrO^{2+}. A DBASLM-impregnated paper strip is also useful for the optical detection of ZrO^{2+}. DBASLM efficiently catalyses the hydrolysis of the phospho-ester bond in *p*-NPP.

Conflicts of interest

We have no conflicts of interest to disclose.

Data availability

Acknowledgements

Notes and references

1 Y. Ma, S. Stopic, X. Wang, K. Forsberg and B. Friedrich, *Metals*, 2020, **10**, 1099–1112.
2 A. S. Amin, *J. Taibah Univ. Sci.*, 2015, **9**, 227–236.
3 S. Ganesh, P. Velavendan, N. K. Pandey, U. K. Mudali and R. Natarajan, *Int. J. Adv. Chem.*, 2015, **1**, 53–59.
4 T.-L. Yau and V. E. Annamalai, *Reference module in materials science and materials engineering*, Elsevier, 2016.
5 D. S. Nakonieczny, A. Ziębowicz, Z. K. Paszenda and C. Krawczyk, *Biocybern. Biomed. Eng.*, 2017, **37**, 229–245.
6 G. Singh, S. Khurana, A. Devi, A. Singh, D. R. Batish and A. Sharma, *Int. J. Biol. Macromol.*, 2024, **261**, 129689.
7 M. Piconi and G. Maccauro, *Biomaterials*, 1999, **20**, 1–25.
8 J. B. Asha and P. Suresh, *ACS Sustainable Chem. Eng.*, 2020, **8**, 14301–14311.
9 A. G. Evanoff and G. Chumanov, *Chem. Rev.*, 2006, **106**, 430–448.
10 S. Ghosh, A. Sharma and G. Talukder, *Biol. Trace Elem. Res.*, 1992, **35**, 247–271.
11 D. B. N. Lee, M. Roberts, C. G. Bluchel and R. A. Odell, *ASAIO J.*, 2010, **56**, 550–556.
12 R. A. Bapat, H. J. Yang, T. V. Chaubal, S. Dharmadhikari, A. M. Abdulla, S. Arora, S. Rawal and P. Kesharwani, *RSC Adv.*, 2022, **12**, 12773–12793.
13 L. Romeo, A. Cazzadori, L. Bontempini and S. Martini, *Med. Lav.*, 1994, **85**, 219–222.

14 E. Bingham, B. Cohrssen and C. H. Powell, *Patty's toxicology*, John Wiley & Sons, New York, 5th edn, 2001, pp. 45–46.

15 K. K. Liippo, S. L. Anttila, O. Taikina-Aho, E.-L. Ruokonen, S. T. Toivonen and T. Tuomi, *Am. Rev. Respir. Dis.*, 1993, **148**, 1089–1092.

16 J. E. Abraham and D. H. Hunt, *Arch. Environ. Health*, 1964, **8**, 627–632.

17 IPCS International Programme on Chemical Safety, Zirconium and its Compounds, UK PID 90, WHO/PCS/INC/95.90.

18 P. A. Curtis, *Contact Dermat.*, 1980, **6**, 319–322.

19 P. L. Currance, B. Clements, and A. C. Bronstein, *Emergency care for hazardous materials exposure*, Mosby, Elsevier, St. Louis, MO, 3rd edn, 2007.

20 D.-E. Zacharioudaki, I. Fitilis and M. Kotti, *Molecules*, 2022, **27**, 4801.

21 L. Y. Kuo, S. Kuhn and D. Ly, *Inorg. Chem.*, 1995, **34**, 5341.

22 H. Morales-Rojas and R. A. Moss, *Chem. Rev.*, 2002, **102**, 2497.

23 J. Fanzo, R. Remans, and P. Sanchez, in *The chemical element: chemistry's contribution to our global future*, ed. J. Garcia-Martinez and E. Serrano-Torregrosa, Wiley-VCH Verlag, Weinheim, 2011.

24 A. N. Bigley and F. M. Raushel, *Chem. Biol. Interact.*, 2019, **308**, 80–88.

25 K. Lai, N. J. Stolowich and J. R. Wild, *Arch. Biochem. Biophys.*, 1995, **318**, 59–64.

26 K. Alejo-González, E. Hanson-Viana and R. Vazquez-Duhalt, *J. Pestic. Sci.*, 2018, **43**, 1–9.

27 E. Dyguda-Kazimierowicz, S. Roszak and W. A. Sokalski, *J. Phys. Chem. B*, 2014, **118**, 7277–7289.

28 I. Mali, C. Shah, B. H. Raghunandan, A. S. Prajapati, D. H. Patel, U. Trivedi and R. B. Subramanian, *J. Environ. Sci.*, 2023, **127**, 234–250.

29 S. Ray and S. T. Shaju, *Environ. Anal. Health Toxicol.*, 2023, **38**, e2023017.

30 C. M. Tomé, M. C. Oliveira, M. Pillinger, I. S. Gonçalves and M. Abrantes, *Dalton Trans.*, 2013, **42**, 3901–3907.

31 A. A. Sari, A. O. Babalghith, R. El-Sayed and A. S. Amin, *Results Chem.*, 2024, **7**, 101513.

32 U. D. Uysal, A. A. Huseyinli and T. Güray, *J. Sci. Ind. Res.*, 2011, **70**, 45–50.

33 T. A. Lasheen, G. Hussein, Y. Khawassek and M. Cheira, *Anal. Chem. Indian J.*, 2013, **12**, 368–376.

34 G. Singh, Heena, S. Khurana, Mithun, B. S. Gill, D. Baliyan, Vikas, N. Dege and E. Tarcan, *Appl. Organomet. Chem.*, 2025, **39**, e7983.

35 D. Marsh, *BioMed Res. Int.*, 2015, **2015**, 746980.

36 W. B. Blumenthal, *J. Chem. Educ.*, 1949, **26**, 472.

37 S. Chatterjee, S. Ta, S. Khanra and D. Das, *RSC Adv.*, 2022, **12**, 33293–33303.

38 T. Shyam, S. Lohar and D. Das, *Inorg. Chim. Acta*, 2025, **583**, 122689.

39 J. Cheng, X. Zhou and H. Xiang, *Analyst*, 2015, **140**, 7082.

40 A. Ashraf, J. M. Herbert, S. Muhammad, B. A. Farooqi, U. Farooq, M. Salman and K. Ayub, *ACS Omega*, 2022, **7**, 2260–2274.

41 Y. Yang, M. N. Weaver and K. M. Merz Jr, *J. Phys. Chem. A*, 2009, **113**, 9843–9851.

42 L. D. Nguyen, T. X. H. Dao, C. T. G. Hua and P. H. Tran, *J. Mol. Liq.*, 2024, **396**, 123859.

43 K. Szentmihályi, S. Klébert, Z. May, E. Bódis, M. Mohai, L. Trif, T. Feczkó and Z. Károly, *Pharmaceutics*, 2022, **14**, 2332.

44 T. Pan, T.-Y. Gao, X.-H. Fan, M.-L. Sa, X.-J. Yang, J.-N. Xu, X. Xu, M. Ma, R. Wang, Y. Zhang, W. Ye, Y.-P. Shi, H.-X. Zhang and Z.-C. Zeng, *Talanta*, 2025, **281**, 126754.

45 T. Shyam, S. Ghosh, S. Maji, P. Mandal and D. Das, *New J. Chem.*, 2023, **47**, 14315–14322.

46 H.-M. Meng, T. Fu, X.-B. Zhang, N.-N. Wang, W. Tan, G.-L. Shen and R.-Q. Yu, *Anal. Chem.*, 2012, **84**, 2124–2128.

47 Z. Liu, Y. Yan, J. Li, W. Zhou, H. Gao and R. Lu, *Anal. Sci.*, 2024, **40**, 1269–1278.

48 M. B. Gholivand, A. Babakhanian and M. Joshaghani, *Anal. Chim. Acta*, 2007, **584**, 302–307.

49 H. A. Arida, *Talanta*, 2008, **76**, 40–43, DOI: 10.1016/j.talanta.2008.01.061.

50 S. T. Frey, B. M. Hutchins, B. J. Anderson, T. K. Schreiber and M. E. Hagerman, *Langmuir*, 2003, **19**, 2188–2192.

51 Y. Zhang, F. Wang, X. Liu, Y. Zhang and J. Liu, *Chem. Rev.*, 2018, **118**, 11618–11705.

52 Q. Zhang, J. Shu, Y. Zhang, Z. Xu, J. Yue, X. Liu, B. Xu, Z. Chen and W. Jiang, *Dalton Trans.*, 2020, **49**, 10261.

53 Z. Liang, K. Liu, Y. Li, Y. Liu, C. Jiang, T. Zhang and W. Chen, *Environ. Sci.: Nano*, 2025, **12**, 1364.